AIChE

Kinetic Insight into Electrochemically Mediated ATRP Gained through Modeling

Jun-Kang Guo, Yin-Ning Zhou, and Zheng-Hong Luo
Dept. of Chemical Engineering, School of Chemistry and Chemical Engineering, Shanghai Jiao Tong University, Shanghai 200240, P.R. China

DOI 10.1002/aic.14969
Published online in Wiley Online Library (wileyonlinelibrary.com)

A detailed kinetic model was constructed using the method of moments to elucidate the electrochemically mediated atom transfer radical polymerization (eATRP). Combined with electrochemical theory, the reducing rate coefficient relevant to the overpotential in eATRP was coupled into the kinetic model. The rate coefficients for eATRP equilibrium and the reducing rate coefficient were fitted to match the experimental data. The effects of catalyst loading, overpotential, and application of programmable electrolysis on the eATRP behavior were investigated based on the tested kinetic model. Results showed that the apparent polymerization rate exhibited a square root dependence on catalyst loading. In addition, a more negative potential accelerated the polymerization rate before the mass transport limitation was reached. This phenomenon indicated that the polymerization rate could be artificially controlled by the designed program (i.e., stepwise and intermittent electrolysis programs). What is more, the normal ATRP, photo-ATRP, and eATRP were compared to obtain a deeper understanding of these ATRP systems. © 2015 American Institute of Chemical Engineers
AIChE J, 00: 000–000, 2015
Keywords: electrochemically mediated ATRP, kinetic model, polymerization mechanism, overpotential

Introduction

Conventional free-radical polymerization is important in the industrial production of polymers because of its wide application in monomers, tolerance to impurities, and economical efficiency compared with other polymerization techniques.[1] Reversible deactivation radical polymerization (RDRP) techniques[2,3] that have been developed in recent years have attracted a great deal of attention because of their good controllability over polymer molecular weight and architectures. These techniques mainly include nitroxide-mediated polymerization,[4] atom-transfer radical polymerization (ATRP),[5] and reversible addition-fragmentation chain-transfer polymerization.[6] However, as one of the most promising RDRP methods, in spite of the huge industrial interest, large-scale ATRP is still limited because it needs large amounts of catalyst (commonly larger than 1000 parts per million [ppm] in conventional ATRP) that has to be removed from the polymer products.[7,8] For industrial application and environmental protection, the level of transition-metal catalyst loading should be reduced as low as possible on the premise of maintaining the ATRP features. Over the past decades, several improved low-concentration catalyst ATRP techniques, in which the concentrations of catalyst had been reduced to as low as 100 or even 50 ppm versus monomer, have been developed. These techniques include initiators for continuous activator regeneration (ICAR) ATRP,[9–12] activators regenerated by electron transfer (ARGET) ATRP,[13–17] supplemental activator and reducing agent (SARA) ATRP,[18–21] photo-induced ATRP (photo-ATRP),[22–25] and electrochemically mediated atom transfer radical polymerization (eATRP).[26–32] These new ATRP systems can regenerate the low-oxidation state activator and polymerize various kinds of monomers with well-defined structure under more environmentally friendly and industrially scalable reaction conditions.

Compared with other ATRPs, the eATRP has distinct characteristics in polymerization controllability. In an eATRP process, the deactivator at the electrode surface turns to an active activator by a single electron reduction process (Scheme 1).[27] Under vigorous stirring, the activator diffuses to the bulk solution, reacts with initiators, and triggers the polymerization reaction. Through the simple alteration of the applied potential, the concentration ratio of the activator and deactivator can be adjusted, resulting in the variation in the polymerization rate, even the polymerization state changes between "on" and "off."[26–31] Additionally, the transition-metal catalyst can be recycled and reused by electrodeposition.[28] Thus, eATRP has been applied to synthesize polymers with well-defined structure. For example, Li et al.[29,30] conducted the controllable polymer brush growth with controllable thickness and architectures by surface-initiated eATRP both on cathode and nonconductive substrates that were terminated by initiators. Park et al.[31] fabricated star polymers using macroinitiators with larger molecular weights and star yield compared with a single step potential by gradually applying more negative potential.

Additional Supporting Information may be found in the online version of this article.

Correspondence concerning this article should be addressed to Z. H. Luo at luozh@sjtu.edu.cn.

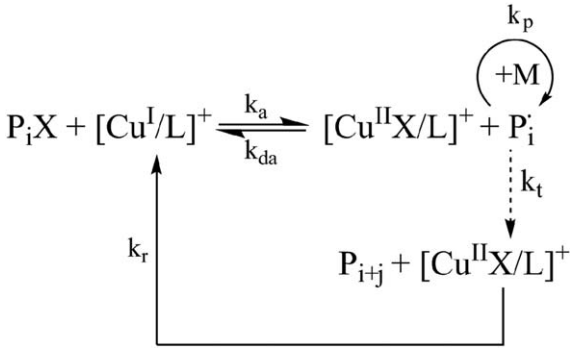

Scheme 1. Mechanism of eATRP.

Kinetic modeling is important in kinetic study as a significant supplemental approach to polymerization engineering. Meanwhile, a well-constructed kinetic model can be used for process prediction, control, optimization, and mechanism study, indicating its significance in chemical engineering.[33–37] Zhu et al.[15,38,39] developed a kinetic model for conventional ATRP based on the method of moments which could successfully predict the evolution of polymerization rate, molecular weight, and polydispersity index with conversion. D'hooge et al.[11,40] and Toloza Porras et al.[12] performed the kinetic modeling of ICAR ATRP using an extended method of moments to control the reaction process. Li et al.[15] and Payne et al.[16,17] optimized the conditions of ARGET ATRP using method of moments and kinetic Monte Carlo method, for example, the ATRP equilibrium coefficient K_{ATRP} (k_a/k_{da}) and the reduction rate coefficient (k_r). In addition, the mechanism of SARA ATRP kinetics was examined by Zhong et al.[19] and Zhou et al.[20] through simulation. More recently, our group made progress in the kinetic modeling of photo-ATRP.[25] However, eATRP kinetic modeling remains ambiguous.

In this work, a comprehensive kinetic modeling was used to describe eATRP to obtain an in-depth understanding of its mechanism and optimize its reaction conditions. The model was based on the method of moments. The variation of all species and reaction rates during polymerization were vividly described, and the efficiency of the proposed model was confirmed through verifying the experimental data, which were based on butyl acrylate (BA) homopolymerization in dimethylformamide (DMF) at 44°C.[28] Meanwhile, the model was used to systematically predict the influence of the catalyst loading, overpotential, and programmable electrolysis on polymerization behavior. Furthermore, the three ATRP methods, namely, normal ATRP, photo-ATRP, and eATRP under their respectively applicable conditions were compared to illustrate their respective polymerization kinetic characteristics qualitatively.

Kinetic Model and Computational Method

Table 1 presents the set of reactions in the simulations. Ethyl 2-bromoisobutyrate (EBiB) is the initiator, and tris(2-pyridylmethyl) amine (TPMA) is the ligand in the polymerization process. From Scheme 1, the deactivator can be reduced to a low-oxidation state activator under the effect of current. Then, the activator reacts with the initiator, and the primary radicals are generated. The other processes, such as chain propagation, activation/deactivation equilibrium, chain transfer, and termination, are similar to those in the normal ATRP, except that the lost activator caused by the persistent radical effect in normal ATRP can be regenerated by electrochemical reduction in eATRP. In addition, for BA homopolymerization, the intramolecular chain transfer (i.e., backbiting) should be considered, which is the dominant mechanism leading to branching compared with intermolecular chain transfer.[44,46] The tertiary radicals produced by backbiting can reversely turn into secondary radicals by addition of monomer. The fragmentation or β-scission of the secondary radicals are neglected under experimental conditions, because the scission reaction is negligible below 75°C.[46,47] Similarly, termination by disproportionation is neglected for simplicity.[12,44] All the relative species in the system, including secondary and tertiary species, or active and dormant species, are in a state of competitive equilibria.[44] It should be noted that diffusion controlled termination plays an important role in radical polymerization at high monomer conversion.[36,40,48–51] However, the experimental data used for kinetic parameter estimation are gained at the conversion lower than 80%, therefore, the influence of diffusion limitation is not taken into account in this work for simplicity.

The mechanism of potential regulation in eATRP is worthy of in-depth studies. When a potential step is applied to the electrode, the effect of concentration polarization must be considered, and the transient mass transfer process can be simplified as a nonsteady diffusion process. Magenau et al.[28] showed that the ratio of peak currents for oxidation and reduction is approximately equal to 1, while the potential difference between the redox peaks is approximately 80 mV. These results indicated that the electrochemical reaction shown in Eq. 1 is a reversible reaction

$$\left[Cu^{II}X/L\right]^{+}+e^{-}\overset{k_{r,e}}{\rightleftharpoons}\left[Cu^{I}/L\right]^{+}+X^{-} \tag{1}$$

This finding is consistent with the results from previous studies.[26,27] According to the electrochemical theory,[52] the nonsteady responding current to the potential step for a reversible system is as follows

$$i(t)=\frac{nFAc_O}{1+\xi\theta}\sqrt{\frac{D_O}{\pi t}} \tag{2}$$

where, n is the number of transfer electron, F is Faraday's constant, and A is the electrode area. D_O and D_R are the diffusion coefficients of high- and low-oxidation state catalysts, respectively. $\xi=\sqrt{\frac{D_O}{D_R}}$ is the square root of the ratio of the two diffusion coefficients, and $\theta=\frac{c_O(x,t)}{c_R(x,t)}=\exp\left[\frac{nF}{RT}\left(\varphi-\varphi^{\Theta'}\right)\right]$ is the concentration ratio of the deactivator and activator. Combined with Faraday's laws of electrolysis, the reduction rate of deactivator can be deduced as Eq. 3[52]

$$\frac{d[Cu^{II}X/L^{+}]}{dt}=\frac{i(t)}{nFV}=\frac{A}{V(1+\xi\theta)}\sqrt{\frac{D_O}{\pi}}\cdot c_O\cdot\sqrt{\frac{1}{t}}=k_r\cdot c_O\cdot\sqrt{\frac{1}{t}} \tag{3}$$

where, the reducing rate coefficient is

$$k_r=\frac{A}{V(1+\xi\theta)}\sqrt{\frac{D_O}{\pi}}. \tag{4}$$

All the rate coefficients used in Table 1 are from the literature, except for those of activation rate, deactivation rate, and reducting rate. In accordance with Konkolewicz et al.'s

Table 1. Elementary Reactions for Normal, Electrochemically Mediated, and Photo ATRP

	Elementary Reaction	Equation	Rate Coefficient[a]	Ref.
Normal ATRP	Initiation	$P_0X+[Cu^I/L]^+ \underset{k_{da0}}{\overset{k_{a0}}{\rightleftharpoons}} P_0^{\cdot}+[Cu^{II}X/L]^+$	2.0×10^3	41
			3.3×10^6	
		$P_0^{\cdot}+M \xrightarrow{k_{in}} P_1^{\cdot}$	2.48×10^4	42
	Propagation (backbiting)	$P_i^{s\cdot}+M \xrightarrow{k_p^s} P_{i+1}^{s\cdot}$	2.48×10^4	42
		$P_i^{s\cdot} \xrightarrow{k_{bb}} P_i^{t\cdot}$	8.2×10^1	43
		$P_i^{t\cdot}+M \xrightarrow{k_p^t} P_{i+1}^{s\cdot}$	2.4×10^2	43
	ATRP equilibrium[b]	$P_i^sX+[Cu^I/L]^+ \underset{k_{da}^s}{\overset{k_a^s}{\rightleftharpoons}} P_i^{s\cdot}+[Cu^{II}X/L]^+$	$(2.0\pm0.1)\times10^2$	This work
			$(2.0\pm0.1)\times10^7$	
		$P_i^tX+[Cu^I/L]^+ \underset{k_{da}^t}{\overset{k_a^t}{\rightleftharpoons}} P_i^{t\cdot}+[Cu^{II}X/L]^+$	2.0×10^2	44
			2.0×10^6	
	Transfer to monomer	$P_i^{s\cdot}+M \xrightarrow{k_{trM}^s} P_i+P_1^{\cdot}$	1.23×10^0	43
		$P_i^{t\cdot}+M \xrightarrow{k_{trM}^t} P_i+P_1^{\cdot}$	5.0×10^{-3}	43
	Termination by recombination[c]	$P_0^{\cdot}+P_0^{\cdot} \xrightarrow{k_{t0}} P_0P_0$	1.1×10^9	45
		$P_0^{\cdot}+P_i^{s\cdot} \xrightarrow{k_{t0}} P_0P_i$	1.1×10^9	45
		$P_0^{\cdot}+P_i^{t\cdot} \xrightarrow{k_{t0}} P_0P_i$	1.1×10^9	45
		$P_i^{s\cdot}+P_j^{s\cdot} \xrightarrow{k_t^{ss}} P_{i+j}$	1.60×10^8	43
		$P_i^{s\cdot}+P_j^{t\cdot} \xrightarrow{k_t^{st}} P_{i+j}$	3.27×10^7	43
		$P_i^{t\cdot}+P_j^{t\cdot} \xrightarrow{k_t^{tt}} P_{i+j}$	2.15×10^6	43
Extra for eATRP	Electrochemical activator (re)generation	$[Cu^{II}X/L]^+ + e^- \xrightarrow{k_{r,e}} [Cu^I/L]^+ + X^-$	$(2.2\pm0.1)\times10^{-3}$	This work
Extra for photo-ATRP	Photochemical radical (re)generation	$Cu^{II}X_2/L+L \xrightarrow{k_{r,C-L}} Cu^IX/L+L^{+\cdot}+X^-$	1.0×10^{-3}	41
		$P_0X+L \xrightarrow{k_{r,I-L}} P_0^{\cdot}+L^{+\cdot}+X^-$	6.2×10^{-6}	41
		$P_rX+L \xrightarrow{k_{r,MT-L}} P_r^{\cdot}+L^{+\cdot}+X^-$	1.4×10^{-6}	41
		$P_0X \xrightarrow{k_{r,I}} P_0^{\cdot}+X^{\cdot}$	2.9×10^{-9}	41
		$M+L \xrightarrow{k_{r,L-M}} M^{-\cdot}+L^{+\cdot}$	1.5×10^{-9}	41

[a]The units for all rate coefficients are $M^{-1}\ s^{-1}$, except that of k_r is expressed in $s^{-1/2}$.
[b]The superscript *s* and *t* represent secondary radicals and tertiary radicals, respectively.
[c]Termination by disproportionation is neglected.

study,[44] the deactivation rate coefficient for tertiary macroradicals was set to 1/10 of that of the secondary one, while both the activation rate coefficients were assumed to be similar, considering the synergistic effect of radical stability and steric effects. Analogously, consistent with Ribelli et al.'s work,[41] the activation and deactivation values in the initiation step, namely, k_{a0} and k_{d0}, respectively, were considered to be ten times and one-sixth that of k_a and k_d, respectively. For the first assumption, with EBiB as initiator and TPMA as ligand in this system, the equilibrium constant K_{ATRP} is set to 1×10^{-5}, which is approximately equal to that reported by Tang et al. (9.65×10^{-6}).[53] Additionally, the reducing rate coefficient is limited in the order of $10^{-4}-10^{-3}\ s^{-\frac{1}{2}}$, which is calculated according to the given experimental parameters. Subsequently, the three rate coefficients, namely, activation, deactivation, and reducing ones, are varied and optimized systematically to mimic the polymerization and fit the experimental data. Thus, a value of $2.0 \times 10^2\ M^{-1}s^{-1}$ for the activation rate coefficient is obtained, which is larger than the value of $1.1 \times 10^2\ M^{-1}s^{-1}$ in anisole using the Arrhenius expression reported by Payne et al.[16] This result is reasonable considering the effect of the solvent on activation.[54,55] Furthermore, the residual analysis is made to test the model outputs as shown in Supporting Information Figure S1. The results indicate that the agreement of simulation predictions with experimental data is fairly good, with the maximum deviation less than 5%.

Table 2 lists the kinetic equations for all species in eATRP according to the elementary reactions. $P_i^{\cdot}$, P_iX, and P_i represent the macroradicals, dormant chains, and dead chains with chain length *i*, respectively. The differential moment equations for the species in eATRP can be listed by defining the moments of chain species, as shown in Tables S1 and S2 in the Supporting Information. In addition, the rates of elementary reactions, concentrations of relative reaction species, and the polymerization properties can be expressed using the moment equations (Eqs. 5–13). Using MATLAB 2009 (b) software, these equations can be used to calculate and output the results.

Table 2. Kinetic Equations for All Species in Electrochemically Mediated ATRP

Type	Mass Balance Equations
Propagating radical chains	$\frac{d[P_i^{s\cdot}]}{dt}=k_p^s[P_{i-1}^{s\cdot}][M]-k_p^s[P_i^{s\cdot}][M]+k_a^s[P_iX][Cu^I/L^+]-k_{da}^s[P_i^{s\cdot}][Cu^{II}X/L^+]-k_{bb}[P_i^{s\cdot}]+k_p^t[P_{i-1}^{t\cdot}][M]-k_{t0}[P_0^{\cdot}][P_i^{s\cdot}]-k_t^{ss}[P_i^{s\cdot}][P_j^{s\cdot}]-k_t^{st}[P_i^{s\cdot}][P_j^{t\cdot}]-k_{trM}^s[P_i^{s\cdot}][M]$
	$\frac{d[P_i^{t\cdot}]}{dt}=k_a^t[P_iX][Cu^I/L^+]-k_{da}^t[P_i^{t\cdot}][Cu^{II}X/L^+]+k_{bb}[P_i^{s\cdot}]-k_p^t[P_i^{t\cdot}][M]-k_{t0}[P_0^{\cdot}][P_i^{t\cdot}]-k_t^{st}[P_i^{t\cdot}][P_j^{s\cdot}]-k_t^{tt}[P_i^{t\cdot}][P_j^{t\cdot}]-k_{trM}^t[P_i^{t\cdot}][M]$
Dormant chains	$\frac{d[P_iX]}{dt}=k_{da}^s[P_i^{s\cdot}][Cu^{II}X/L^+]-k_a^s[P_iX][Cu^I/L^+]$
	$\frac{d[P_i^tX]}{dt}=k_{da}^t[P_i^{t\cdot}][Cu^{II}X/L^+]-k_a^t[P_i^tX][Cu^I/L^+]$
Dead chains	$\frac{d[P_i]}{dt}=k_{t0}[P_0^{\cdot}]([P_i^{s\cdot}]+[P_i^{t\cdot}])+\frac{1}{2}\sum_{j=1}^{i}k_t^{ss}[P_j^{s\cdot}][P_{i-j}^{s\cdot}]+\frac{1}{2}\sum_{j=1}^{i}k_t^{st}[P_j^{s\cdot}][P_{i-j}^{t\cdot}]+\frac{1}{2}\sum_{j=1}^{i}k_t^{tt}[P_j^{t\cdot}][P_{i-j}^{t\cdot}]$
Monomer	$\frac{d[M]}{dt}=-k_{in}[P_0^{\cdot}][M]-k_p^s[P_i^{s\cdot}][M]-k_p^t[P_i^{t\cdot}][M]-k_{trM}^s[P_i^{s\cdot}][M]-k_{trM}^t[P_i^{t\cdot}][M]$
Initiator	$\frac{d[P_0X]}{dt}=k_{da,0}[Cu^{II}X/L^+][P_0^{\cdot}]-k_{a,0}[Cu^I/L^+][P_0X]$
Primary radical	$\frac{d[P_0^{\cdot}]}{dt}=-k_{in}[P_0^{\cdot}][M]+k_{a,0}[Cu^I/L^+][P_0X]-k_{da,0}[Cu^{II}X/L^+][P_0^{\cdot}]-2k_{t0}[P_0^{\cdot}][P_0^{\cdot}]-k_{t0}[P_0^{\cdot}]([P_i^{s\cdot}]+[P_i^{t\cdot}])$
Activator	$\frac{d[Cu^I/L]}{dt}=k_{da,0}[Cu^{II}X/L^+][P_0^{\cdot}]-k_{a,0}[Cu^I/L^+][P_0X]+k_{da}^s[Cu^{II}X/L^+][P_i^{s\cdot}]-k_a^s[Cu^I/L^+][P_iX]+k_{da}^t[Cu^{II}X/L^+][P_i^{t\cdot}]-k_a^t[Cu^I/L^+][P_i^tX]+f(t)$
Deactivator	$\frac{d[Cu^{II}X/L^+]}{dt}=-k_{da,0}[Cu^{II}X/L^+][P_0^{\cdot}]+k_{a,0}[Cu^I/L^+][P_0X]-k_{da}^s[Cu^{II}X/L^+][P_i^{s\cdot}]+k_a^s[Cu^I/L^+][P_iX]-k_{da}^t[Cu^{II}X/L^+][P_i^{t\cdot}]+k_a^t[Cu^I/L^+][P_i^tX]-f(t)$

Reaction rates

The reaction rates are as follows

$$R_p^s=k_p^s\left[P_i^{s\cdot}\right][M] \tag{5}$$

$$R_p^t=k_p^t\left[P_i^{t\cdot}\right][M] \tag{6}$$

$$R_a^s=k_a^s\left[P_iX\right]\left[Cu^I/L^+\right] \tag{7}$$

$$R_{da}^s=k_{da}^s\left[P_i^{s\cdot}\right]\left[CuX^{II}/L^+\right] \tag{8}$$

$$R_{bb}=k_{bb}\left[P_i^{s\cdot}\right] \tag{9}$$

$$R_a^t=k_a^t\left[P_i^tX\right]\left[Cu^I/L^+\right] \tag{10}$$

$$R_{da}^t=k_{da}^t\left[P_i^{t\cdot}\right]\left[CuX^{II}/L^+\right] \tag{11}$$

$$R_{tr,M}=k_{trM}^s\left[P_i^{s\cdot}\right][M]+k_{trM}^t\left[P_i^{t\cdot}\right][M] \tag{12}$$

$$R_t=k_{t0}[P_0^{\cdot}]\left([P_0^{\cdot}]+\left[P_i^{s\cdot}\right]+\left[P_i^{t\cdot}\right]\right)+k_t^{ss}\left[P_i^{s\cdot}\right]\left[P_j^{s\cdot}\right]+k_t^{tt}\left[P_i^{t\cdot}\right]\left[P_j^{t\cdot}\right]+k_t^{st}\left[P_i^{s\cdot}\right]\left[P_j^{t\cdot}\right] \tag{13}$$

The number-average molecular weight (M_n) is as follows

$$M_n=\overline{M}_{\text{monomer}}\frac{\sum\left(\lambda^{s,1}+\lambda^{t,1}+\mu^{s,1}+\mu^{t,1}+\tau^1\right)}{\sum\left(\lambda^{s,0}+\lambda^{t,0}+\mu^{s,0}+\mu^{t,0}+\tau^0\right)} \tag{14}$$

The weight-average molecular chain length (M_w) is as follows

$$M_w=\overline{M}_{\text{monomer}}\frac{\sum\left(\lambda^{s,2}+\lambda^{t,2}+\mu^{s,2}+\mu^{t,2}+\tau^2\right)}{\sum\left(\lambda^{s,1}+\lambda^{t,1}+\mu^{s,1}+\mu^{t,1}+\tau^1\right)} \tag{15}$$

The molecular weight distribution (M_w/M_n) is calculated as follows

$$M_w/M_n=\frac{\sum\left(\lambda^{s,2}+\lambda^{t,2}+\mu^{s,2}+\mu^{t,2}+\tau^2\right)\cdot\sum\left(\lambda^{s,0}+\lambda^{t,0}+\mu^{s,0}+\mu^{t,0}+\tau^0\right)}{\left[\sum\left(\lambda^{s,1}+\lambda^{t,1}+\mu^{s,1}+\mu^{t,1}+\tau^1\right)\right]^2} \tag{16}$$

The chain-end functionality (F_t) is determined as follows

$$F_t=\frac{\lambda^{s,0}+\lambda^{t,0}}{\sum\left(\lambda^{s,0}+\lambda^{t,0}+\mu^{s,0}+\mu^{t,0}+2\tau^0\right)} \tag{17}$$

Results and Discussion

Concentrations of reactants and rates of reactions for eATRP

According to the built model, the time-dependent concentrations of all species and rates of reactions using rate

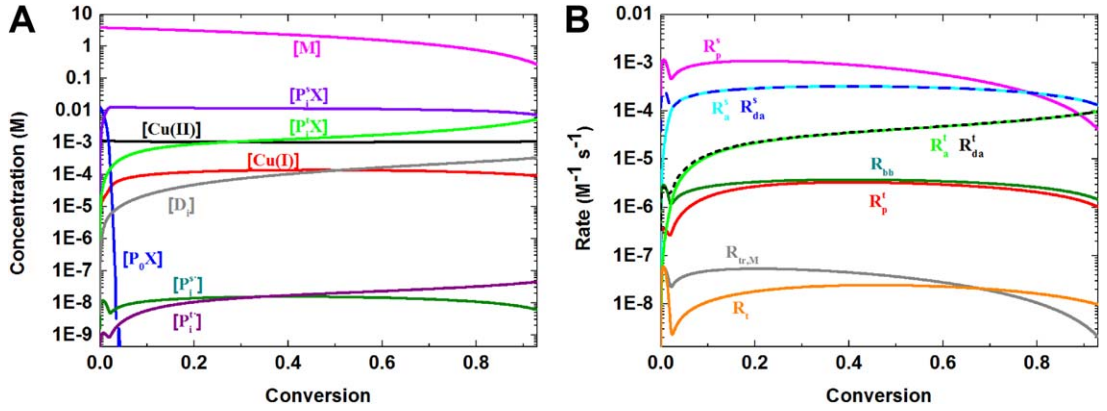

Figure 1. Evolution of reactant concentrations (A) and reaction rates (B) for eATRP of BA.

[Color figure can be viewed in the online issue, which is available at wileyonlinelibrary.com.]

coefficients listed in Table 1 are determined under the following polymerization conditions: $[BA]_0$:$[EBiB]_0$:$[Br\text{-}Cu^{II}TPMA^+]_0$, 300:1:0.09; BA, 3.9 M in DMF; and T, 44°C. The results are shown in Figure 1.

During eATRP, as soon as the potential step is applied, the deactivator near the electrode is reduced, then diffuses to the reaction mixture, reacts with initiators, and triggers the polymerization reaction. In agreement with the characteristic of current responding to the potential step, that is, exponential decay in the current with the square root of time, the concentration of activator reaches a constant level of 10^{-4} M^{-1} at the beginning of polymerization. This characteristic indicates a large reducing rate during the initial period of polymerization. Therefore, the induction period for eATRP is very short. Along with the fast production of activator, the initiator is depleted in a short time (Figure 1A). Note that the generation of primary radicals should be accompanied with the decomposition of initiator, resulting in large reaction rates related to primary radicals, for example, R_p, R_{da}, and especially that of termination, R_t. The large amounts of radicals introduced by fast activation should lead to enhanced termination, which is a universal characteristic for RDRP (Figure 1B). With progressively decreasing primary radicals, these rate items gradually slow down and reach a relatively stable state. For BA polymerization in this system, the formation rate of tertiary radicals (R_{bb}) is slightly larger than its consumption rate (R_p^t), leading to the accumulation of tertiary species (including dormant and active species) while reducing the secondary species (Figure 1A). Given that the rate coefficient for propagation of secondary radicals is two orders of magnitude higher than that of tertiary radicals, the apparent propagation rate largely depends on the concentration of the secondary radicals (Eq. 18). Thus, the apparent propagation rate would drop off, especially at high conversion as concentration of monomer also decreases

$$R_p = R_p^s + R_p^t = k_p^s[M][P_i^{s\bullet}] + k_p^t[M]\left[P_i^{t\bullet}\right] \approx k_p^s[M][P_i^{s\bullet}] \quad (18)$$

However, due to the deactivation effect of the deactivator, the concentration of the dormant species (mainly, secondary dormant species) remains nearly constant during the whole reaction, which indicates a low-level termination. This point can also be verified by the proportion of dead chains in the total polymer chains, which is as low as 3% at the last period of polymerization. Moreover, the ATRP equilibria of the secondary and dormant species are established as soon as the initiator become exhausted, which can be deduced from the almost similar values of activation and deactivation rates. Thus, detailed information on eATRP is represented vividly, which is of great help for the better understanding of the reaction mechanism.

Effect of catalyst loading on the eATRP behavior

The amount of catalyst loading has always been the chief concern because it is the major barrier to the industrialization of ATRP. Figure 2 depicts the effect of initial catalyst loading on the semilogarithmic kinetic plot and evolutions of M_n, M_w/M_n, and end functionality with conversion. The simulation is verified by accessible experimental data from Magenau et al.[28] and made further predictions for thorough comprehension.

As seen in Figure 2, the fitting curves are in good agreement with the experimental data. Figure 2A shows a significant positive correlation between the polymerization rate and catalyst loading, that is, faster polymerization with higher Cu level. In fact, the value of $\ln[(M)_0/(M)_t]$ grows linearly as time increases until the conversion reaches about 80% ($\ln[(M)_0/(M)_t] = 1.6$), in agreement with experimental data.[28] Regardless of the decrease at high monomer conversion, the apparent polymerization rate has a square root-dependence on catalyst loading as shown in Figure S2 in the Supporting Information. With larger initial catalyst loading, the amount of activator that can be electrochemically reduced is higher, implying faster polymerization.

However, decreasing the amount of catalyst loading leads to the increases in M_n and M_w/M_n at low monomer conversion (see Figures 2B, C). When a high-oxidation state catalyst of 25 ppm is loaded, for example, most of them will be rapidly reduced to low-oxidation state activator as the current is large at the beginning period of electrolysis. As a result, the system becomes close to normal ATRP at low conversion because of the insufficiency of deactivation from deactivator. Thus, the controllability over the polymerization system weakens at low catalyst concentration, which is analogous to the results found in the studies of ARGET ATRP.[17,56] Remarkably, experimental values of M_n are not increasing linearly with conversion and there is a deviation in high conversion as shown in Figure 2B, which implies that the initiator efficiency (the ratio of theoretical M_n and experimental M_n) is more than 100%. In other word, there is an increase of the total number of polymer chains in the system. In theory, only massive chain transfer in the elementary reactions increases the total number of polymer chains, that is, zero-order moments, and consequently can decrease the value of M_n. Herein, the chain-transfer coefficient

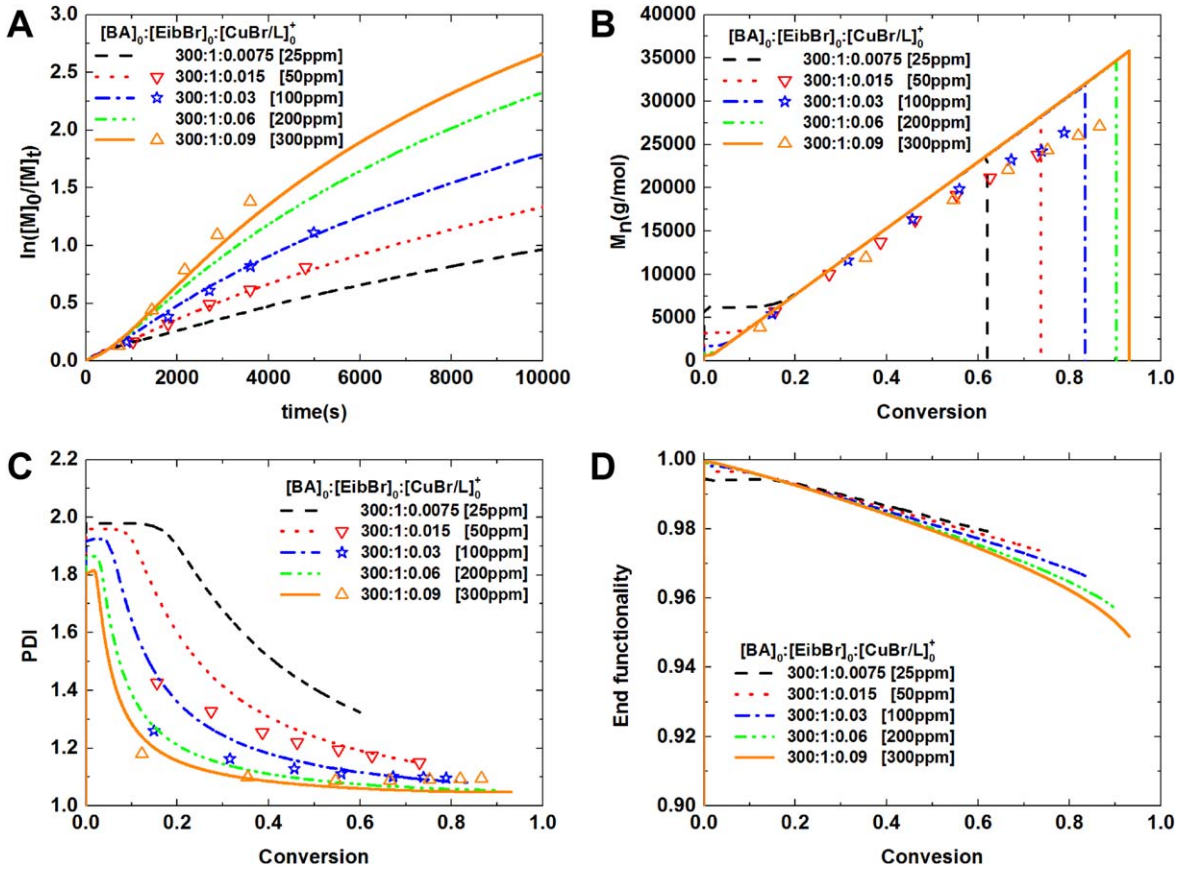

Figure 2. Comparison of kinetic experimental data (points) and simulation results (lines) under different catalyst concentrations: (A) semilogarithmic kinetic plot; (B) evolution of M_n with conversion; (C) evolution of M_w/M_n with conversion; (D) evolution of end functionality with conversion.

[Color figure can be viewed in the online issue, which is available at wileyonlinelibrary.com.]

is expanded by 50 times, and the simulation results become in agreement with experimental data as seen in Supporting Information Figure S3. However, the value of end functionality dramatically decreases to 0.4 in 10,000 s, which is inconsistent with the characteristic of ATRP. Conversely, of course, arbitrary expanding of chain-transfer coefficient is without a scientific reason. Instead, it is notable that the values of M_n were determined by gel permeation chromatography (GPC) using polystyrene as standard sample in the original literature.[28] The GPC measurement is not always precise and the deviation of simulation results from experimental data is likely caused by experimental error. Besides, similar to other ATRP systems, eATRP can hardly maintain the ability to mediate polymer chains well while using catalysts lower than a certain threshold value.[16] When the catalyst loading is set to 25 ppm, only 60% of the monomers are polymerized, and the value of M_w/M_n is as high as 1.3 in 10,000 s. Supporting Information Figure S4 shows that 80,000 s are required to achieve a relatively steady M_w/M_n value of 1.2, which is still higher than the one shown in Figure 2C at 50 ppm.

In addition, the simulations also demonstrate the decrease in the end functionality with increasing catalyst concentration, as reported by Wang et al.[57] The loss of end functionality is mainly caused by the termination according to the kinetic model, which is dependent on the active species. Thus, the higher is the catalyst loading, the less preserved is the end functionality. Nonetheless, even if the largest catalyst loading (300 ppm) is used, more than 94% of the polymer chains exist as dormant species at the end of polymerization as shown in Figure 2D, suggesting an excellent "living" property.

Effect of the Overpotential on the eATRP Behavior. From Eq. 2, with the varying potential applied on the electrode, the responding current-time curves are similar in shape, except for the magnitude scaled by the factor $(\frac{1}{1+\xi\theta})$. When a highly negative potential is applied, the reaction rate is totally controlled by diffusion. This characteristic indicates that the deactivator is reduced the moment it diffuses to the electrode surface from the bulk solution. At this point, the parameter θ approaches zero, and Eq. 2 can be simplified as the Conttrell Equation.[48] The polymerization reaches its maximum rate at $\eta=-0.165$ V because of the mass transport limitations,[28] at which the Conttrell Equation can be approximately used.

Combining the developed model and experimental data at $\eta=-0.165$ V, the maximum reducing rate coefficient can be extrapolated as $k_{r\max}=\frac{A}{V}\sqrt{\frac{D_O}{\pi}}=2.57\times10^{-3}\mathrm{s}^{-1/2}$. Substituting the two reducing coefficient values of $\eta=-0.165$ and -0.125 V into Eq. 4, and the reducing rate coefficient of an arbitrary overpotential value can be derived (Eq. 19). For example, the reducing rates under overpotentials of -0.045, -0.065, -0.085, and -0.105 V are calculated as 0.62, 1.02, 1.49, and 1.90 $\mathrm{s}^{-1/2}$, respectively. These values are used in the following study of the overpotential to polymerization behavior

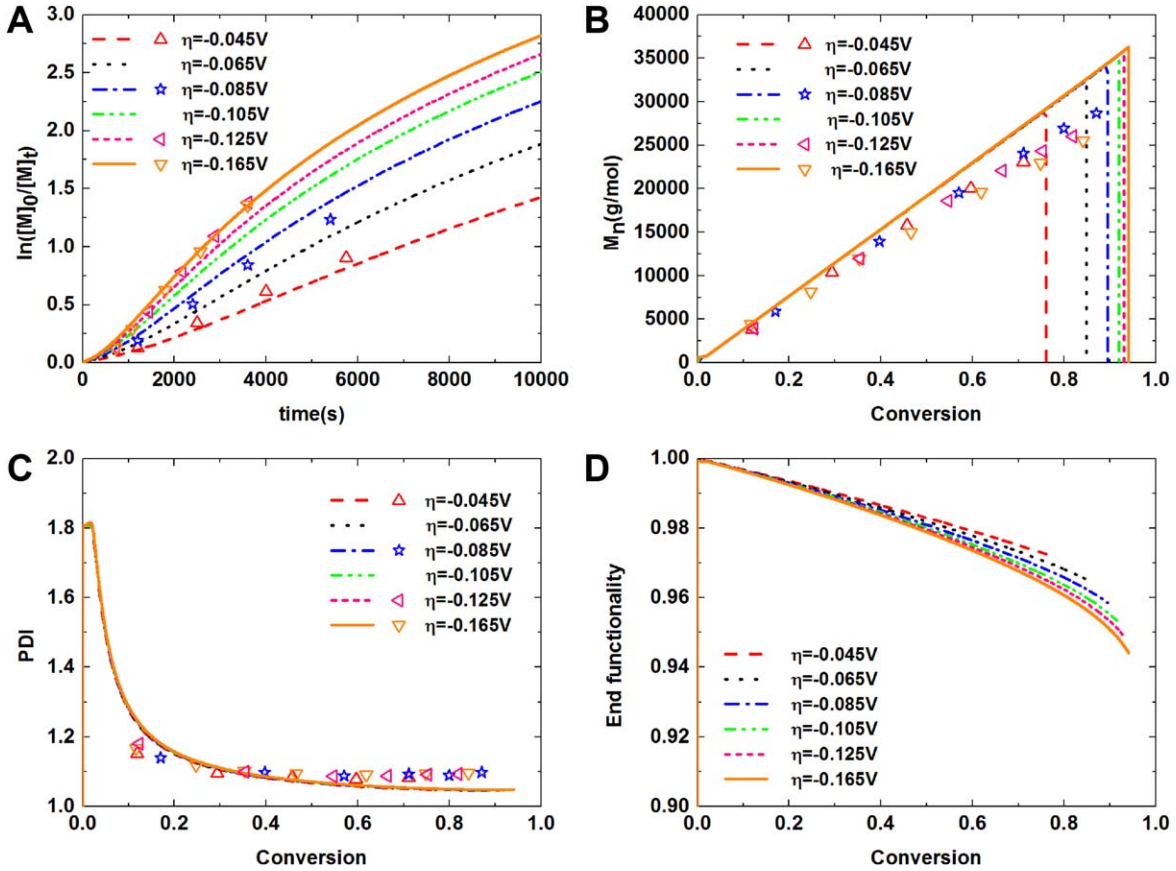

Figure 3. Comparison of kinetic experimental data (points) and simulation results (lines) under different overpotentials: (A) semilogarithmic kinetic plot; (B) evolution of M_n with conversion; (C) evolution of M_w/M_n with conversion; (D) evolution of end functionality with conversion.

[Color figure can be viewed in the online issue, which is available at wileyonlinelibrary.com.]

$$k_{r(\varphi)} = \frac{k_{r\max}}{1+\left(\frac{k_{r\max}}{k_{r(-0.125)}}-1\right)\cdot\exp\left[\frac{nF}{RT}(\varphi+0.125)\right]} \tag{19}$$

Accordingly, the significance of the overpotential on polymerization can be quantified by substituting the reducing rate coefficient derived from Eq. 19 into the kinetic model.

The significance of overpotential is depicted in Figure 3 by modeling eATRP under varying overpotential from −0.045 to −0.165 V with otherwise identical formulations: $[BA]_0$:$[EBiB]_0$:$[Br\text{-}Cu^{II}TPMA^+]_0 = 300{:}1{:}0.09$. Figures 3A to 3C show that the developed kinetic model fit the experimental data well, matching the gradual increase in polymerization rate with more negative potential. Hence, with identical catalyst loadings, the generation rate of activator increases with the overpotential, which is similar to the polymerization rate. However, although enhanced polymerization is observed with larger overpotential, the gradient becomes smaller. To show the relationship between overpotential and polymerization rate, a semilogarithmic plot of k_{app} versus η is illustrated in the Supporting Information. As shown in Supporting Information Figure S5, with the same 0.04 V more negative potential, the apparent polymerization rate grows approximately by 73% from −0.045 to −0.085 V, while minimal change is obtained from −0.125 to −0.165 V. This finding suggests the transformation of the reduction rate-limiting step from hybrid control to complete the diffusion control. Figures 3B, C provide the evolution of M_n and M_w/M_n with conversion. The linear increase in the M_n with monomer conversion and low M_w/M_n values for all cases prove the controllability of this polymerization system. Moreover, M_w/M_n values are nearly unchanged for systems operating at different overpotentials, which can provide an important reference for polymer preparation. Before mass transport limitation is reached, the apparent polymerization rate increases at a near-linear trend as seen in Supporting Information Figure S5. This phenomenon implies that with more negative potential, the production efficiency is higher, while the M_w/M_n values, as one of the main polymer product quality indices, remain stable.

Application of the Programmable Overpotentialon the eATRP Behavior. The overpotential applied has a major impact on reducing rate, thus affecting the polymerization kinetics. This characteristic facilitates the modulation of the rate of polymerization by programmable changing of the potential applied on the electrode.

Figures 4 and 5 show the application of programmable change in the overpotential on eATRP behavior under the condition that $[BA]_0$:$[EBiB]_0$:$[Br\text{-}Cu^{II}TPMA^+]_0 = 300{:}1{:}0.09$ using stepwise and intermittent electrolyses, respectively. Under stepwise electrolysis, the overpotential applied is changed every 2500 s, from −0.045 to −0.125 V (Figure 4). With the increase in overpotential, the apparent propagation rate increases remarkably, which coincides with the previous finding. Using a potential step of −0.125 V at high

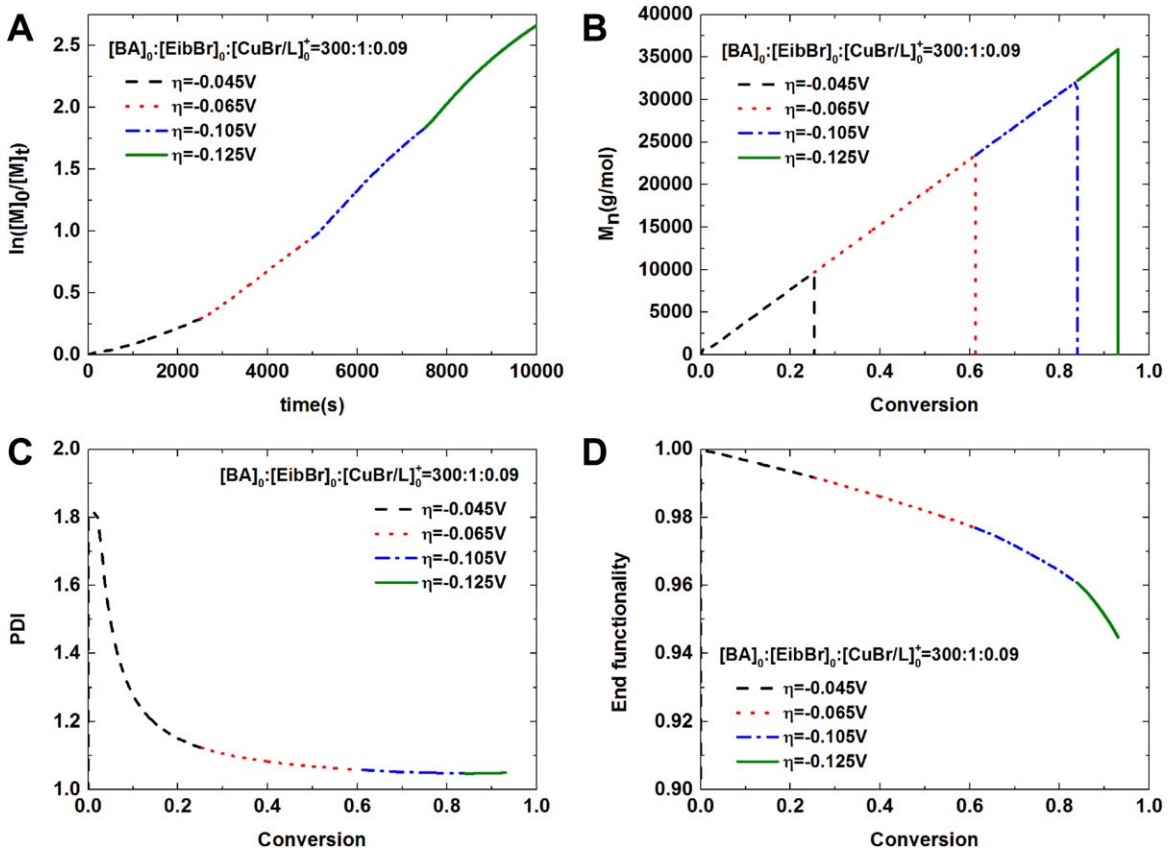

Figure 4. Simulation of eATRP using stepwise electrolysis: (A) semilogarithmic kinetic plot; (B) evolution of M_n with conversion; (C) evolution of M_w/M_n with conversion; (D) evolution of end functionality with conversion.

[Color figure can be viewed in the online issue, which is available at wileyonlinelibrary.com.]

conversion, the concentration ratio of low-oxidation state activator and high-oxidation state deactivator increases according to Nernst equation, as a result of which the ATRP equilibrium moves to active species direction. And the apparent propagation rate expressed as Eq. 20 is maintained at high level

$$\ln\left(\frac{[M]_0}{[M]_t}\right)=k_p[P_i^{\cdot}]t=\frac{k_pK_{\mathrm{ATRP}}[P_iX][Cu^I/L^+]}{[Cu^{II}X/L^+]}t \qquad (20)$$

Thus, those cases where the polymerization rates decrease caused by accumulation of tertiary species (Figure 3) are avoided. Compared with the case in which an overpotential of −0.045 V is used during the whole reaction, the conversion has increased from 76% to 93% in similar time. Additionally, the steady value of M_w/M_n very slightly changes, being consistent with the conclusion that overpotential slightly influence on the M_w/M_n value. And the end functionality also keeps preserved well.

However, the application of intermittent electrolysis is also studied by controlling the electrolytic switch at "on" and "off" with overpotential of −0.125 V at intervals. Figure 5A shows the detailed operation steps, where the gray zone represents the "power off." The system is electrolyzed to produce initial active species in the first stage of 2000 s when the system gets into a steady state. Then, the electrolytic switch is turned off, and polymerization acts like a normal ATRP system, in which the polymerization rate decreases with the conversion because of the persistent radical effect. Thus, the differences between normal ATRP and eATRP are presented visually, contributing to the understanding of the mechanism of eATRP. After 2000 s, the concentration of macroradicals is reduced to 7.7×10^{-5} M, about half of the value in the steady state, and the polymerization rate decreased obviously. Given the residual radicals, 1000 s is sufficient for the following electrolytic procedure for "reactivating" the system. These steps are repeated until 10,000 s (Figure 5). The results indicate that the ultimate conversions by intermittent and continuous electrolysis are almost the same (Figures 3 and 5). This phenomenon suggests that, in spite of shorter time, intermittent electrolysis can offer comparable polymer products comparing with continuous electrolysis. This result is probably due to the much higher amount of activator generated at the beginning of each potential step than that generated during steady state. Hence, the average concentration levels of low-oxidation state catalyst for both electrolysis methods during the whole reaction are likely the same, leading to similar apparent propagation rates. Moreover, compared with constant potential electrolysis, the features of evolutions of M_n, M_w/M_n, and end functionality with conversion (Figures 5B, D) keep almost unchanged, suggesting that the good controllability over the eATRP system is still preserved. Therefore, a new concept and a new method are provided for the controllable and effective preparation of polymers by well-designed electrolysis programs.

Comparison of normal ATRP, photo-ATRP, and eATRP

The eATRP utilizes current to reduce high-oxidation state catalyst, whereas photo-ATRP uses photochemical reduction effect, both of which omit the chemical reducing agent used in other improved ATRPs. Hence, distinguishing the normal ATRP, photo-ATRP, and eATRP to better understand their

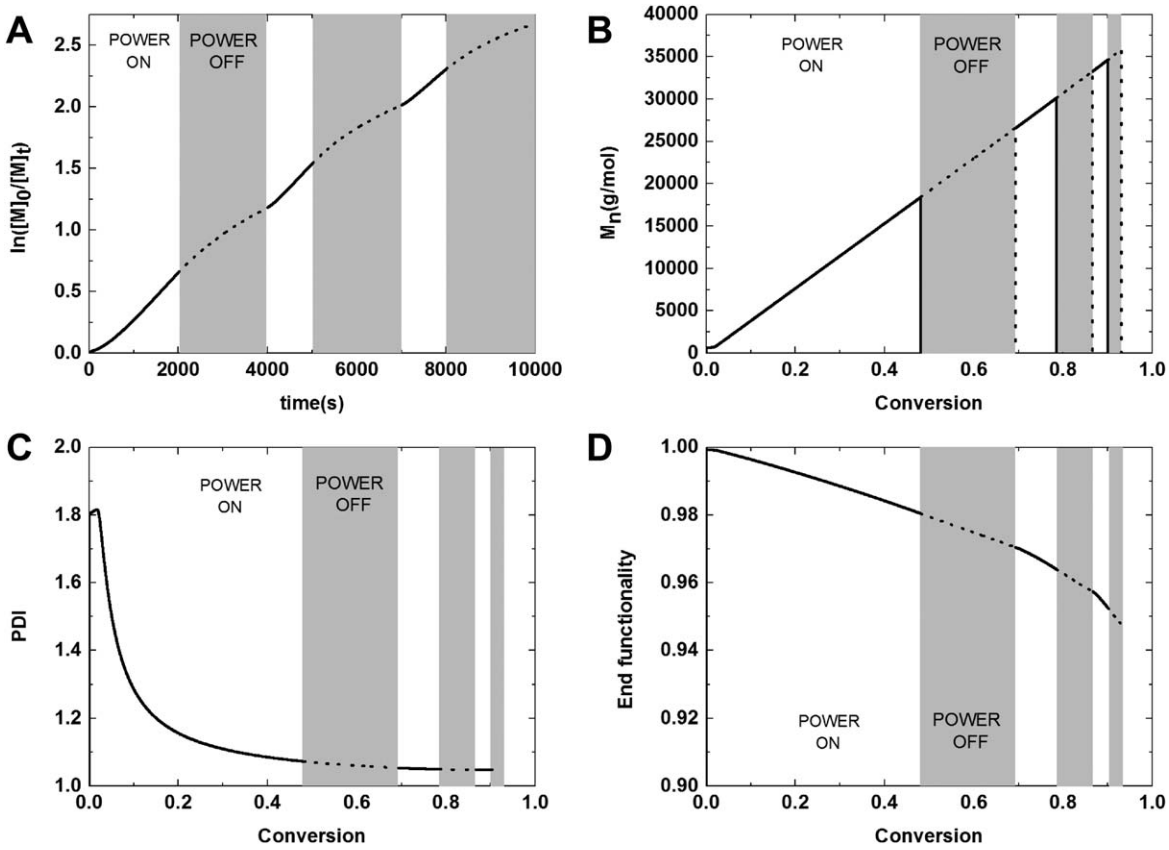

Figure 5. Simulation of eATRP using intermittent electrolysis: (A) semilogarithmic kinetic plot; (B) evolution of M_n with conversion; (C) evolution of M_w/M_n with conversion; (D) evolution of end functionality with conversion.

respective characteristics is important. Herein, given that we have developed the normal and photo-ATRP models for the same polymerization system, these models are applied directly in this work.[25,58] Furthermore, the comparison is performed under their respectively applicable conditions to illustrate their respective polymerization characteristics qualitatively.

Figure 6 shows the simulation results of the three types of ATRP. The simulation of eATRP proceeds under the condition of $[BA]_0$:$[EBiB]_0$:$[Br\text{-}Cu^{II}TPMA^+]_0 = 300$:1:0.09 with overpotential of −0.125 V. The photo-ATRP polymerization behavior is simulated under identical concentration of catalyst with 392 nm UV light irradiation, whereas normal ATRP uses typical condition with equal amounts of initiator and catalyst, that is, $[BA]_0$:$[EBiB]_0$:$[Br\text{-}Cu^{I}TPMA]_0 = 300$:1:1. Figure 6A demonstrates that the polymerization rate of normal ATRP is much faster compared with the other two methods at the beginning of reaction, which could be attributed to the large amount of low-oxidation state catalyst. The drawback of a fast reaction rate is the loss of controllability. The simulation clearly confirms this point that the end functionality has a much smaller initial value and drops quickly compared with others. This finding is due to the high concentration level of the active species and high resultant termination. The evolution of M_n with conversion as shown by Figure 6B also supports this view. The slope in Figure 6B is obviously larger than those of improved ATRP, which implies the loss of halogen groups. Additionally, the M_w/M_n for normal ATRP (Figure 6C) is also higher than those of the other ATRPs. Photo-ATRP and eATRP have many common characteristics, such as low M_w/M_n value and high end functionality (Figure 6D), except that the polymerization rate of eATRP is faster than that of photo-ATRP. This finding can be explained by the difference in the reducing rates of the two methods. Therefore, photo-ATRP and eATRP, as improved ATRPs that utilize external regulation without extra addition of chemical reducing agent, share similar characteristics to some extent and have significant advantages over normal ATRP.

Conclusion

Hence, a detailed kinetic model of eATRP was developed using the method of moments. According to the electrochemical theory, the way by which potential step affected the activator (re)generation was investigated and coupled into the model. Combined with previously published data, three rate coefficients, namely, activation, deactivation, and reducing rate coefficients, were systematically investigated to match the experimental data. The unique features of eATRP were vividly presented by the evolution of reactants and rates of reaction for BA polymerization. For example, the reducing rate decay with the square root of time was very fast, leading to fast termination at the beginning of the reaction. However, the intramolecular chain transfer (backbiting) of BA caused the accumulation of tertiary macroradicals, the propagation rate of which was much slower than secondary ones. Additionally, the simulations on the effect of catalyst loading, overpotential, and application of programmable electrolysis on ATRP behavior were investigated. The results indicated that the apparent polymerization rate had a square root-dependence on the catalyst loading. Before the mass transport limitation is reached, a

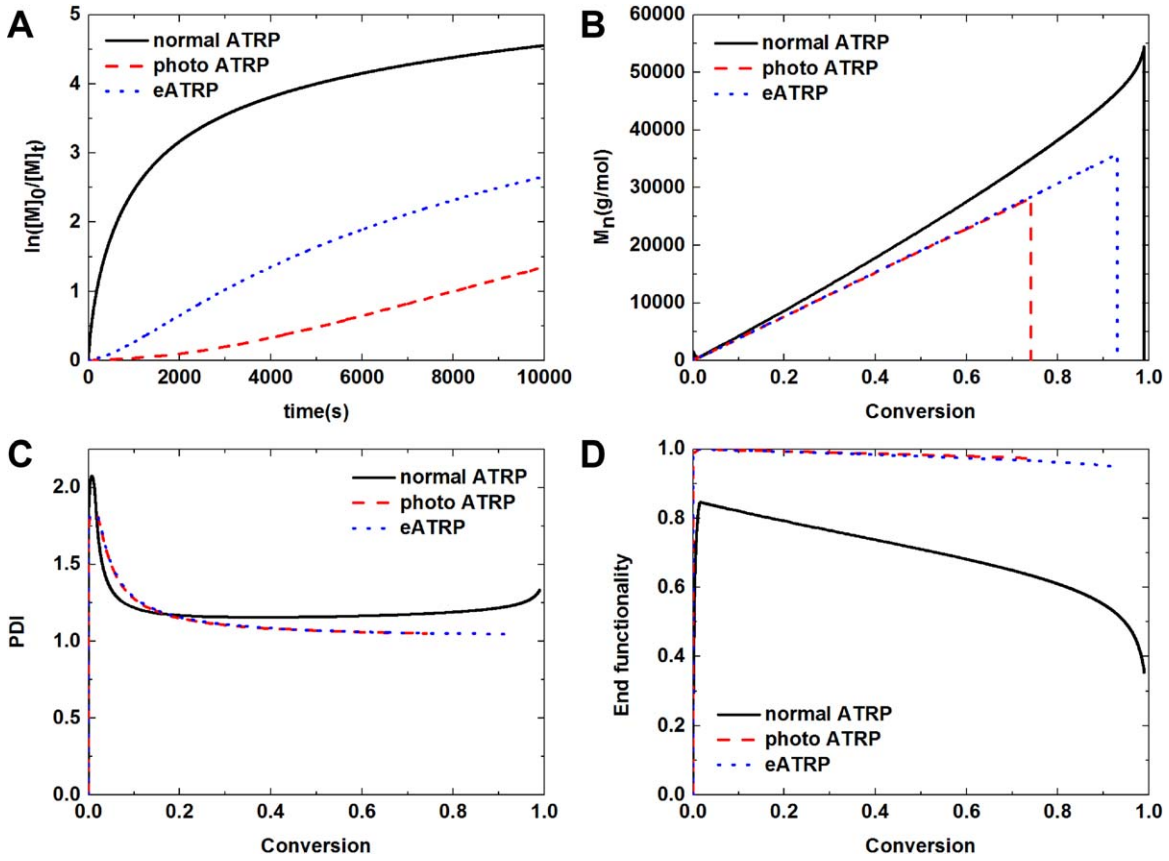

Figure 6. Simulation of three types of ATRP under respectively typical conditions: (A) semilogarithmic kinetic plot; (B) evolution of M_n with conversion; (C) evolution of M_w/M_n with conversion; (D) evolution of end functionality with conversion.

[Color figure can be viewed in the online issue, which is available at wileyonlinelibrary.com.]

more negative potential can accelerate the polymerization rate. Based on this finding, stepwise and intermittent electrolysis programs were designed. The results showed that the polymerization rate can be artificially controlled by different designed programs. Finally, the differences among normal ATRP, photo-ATRP, and eATRP under typical conditions were also examined to better understand their respective characteristics. Considering the large amount of low-oxidation state catalyst, the normal ATRP exhibited a large propagation rate but high loss of end functionality while photo-ATRP and eATRP have no significant differences in polymerization behavior.

Acknowledgment

The authors thank the National Natural Science Foundation of China (No. 21276213) and the National High Technology Research and Development Program of China (No. 2013AA032302) for supporting this work.

Literature Cited

1. Chatgilialoglu C, Studer A. Encyclopedia of radicals in chemistry, biology and materials. In: Nesvadba P, editor. *Radical Polymerization in Industry*. New York: Wiley, 2012:1701–1736.
2. Goto A, Fukuda T. Kinetics of living radical polymerization. *Prog Polym Sci*. 2004;29:329–385.
3. Braunecker WA, Matyjaszewski K. Controlled/living radical polymerization: features, developments, and perspectives. *Prog Polym Sci*. 2007;32:93–146.
4. Nicolas J, Guillaneuf Y, Lefay C, Bertin D, Gigmes D, Charleux B. Nitroxide-mediated polymerization. *Prog Polym Sci*. 2013;38:63–235.
5. Matyjaszewski K. Atom transfer radical polymerization (ATRP): current status and future perspectives. *Macromolecules*. 2012;45:4015–4039.
6. Moad G, Rizzardo E, Thang SH. Living radical polymerization by the RAFT process–a third update. *Aust J Chem*. 2012;65:985–1076.
7. Destarac M. Controlled radical polymerization: industrial stakes, obstacles and achievements. *Macromol React Eng*. 2010;4:165–179.
8. Matyjaszewski K, Jakubowski W, Min K, Tang W, Huang J, Braunecker WA, Tsarevsky NV. Diminishing catalyst concentration in atom transfer radical polymerization with reducing agents. *Proc Natl Acad Sci USA*. 2006;103:15309–15314.
9. Konkolewicz D, Magenau AJD, Averick SE, Simakova A, He H, Matyjaszewski K. ICAR ATRP with ppm Cu catalyst in water. *Macromolecules*. 2012;45:4461–4468.
10. Mueller L, Jakubowski W, Tang W, Matyjaszewski K. Successful chain extension of polyacrylate and polystyrene macroinitiators with methacrylates in an ARGET and ICAR ATRP. *Macromolecules*. 2007;40:6464–6472.
11. D'hooge DR, Konkolewicz D, Reyniers M-F, Marin GB, Matyjaszewski K. Kinetic modeling of ICAR ATRP. *Macromol Theory Simul*. 2012;21:52–69.
12. Toloza Porras C, D'hooge DR, Reyniers M-F, Marin GB. Computer-aided optimization of conditions for fast and controlled ICAR ATRP of n-Butyl Acrylate. *Macromol Theory Simul*. 2013;22:136–149.
13. Jakubowski W, Matyjaszewski K. Activators regenerated by electron transfer for atom-transfer radical polymerization of (meth)acrylates and related block copolymers. *Angew Chem Int Ed*. 2006;45:4482–4486.
14. Dong H, Matyjaszewski K. ARGET ATRP of 2-(dimethylamino)ethyl methacrylate as an intrinsic reducing agent. *Macromolecules*. 2008;41:6868–6870.

15. Li X, Wang WJ, Li BG, Zhu S. Kinetics and modeling of solution ARGET ATRP of styrene, butyl acrylate, and methyl methacrylate. *Macromol React Eng*. 2011;5:467–478.
16. Payne KA, D'Hooge DR, Van Steenberge PHM, Reyniers MF, Cunningham MF, Hutchinson RA, Marin GB. ARGET ATRP of butyl methacrylate: utilizing kinetic modeling to understand experimental trends. *Macromolecules*. 2013;46:3828–3840.
17. Payne KA, Van Steenberge PHM, D'hooge DR, Reyniers M-F, Marin GB, Huthinson RA, Cunningham MF. Controlled synthesis of poly [(butyl methacrylate)-co-(butyl acrylate)] via activator regenerated by electron transfer atom transfer radical polymerization: insights and improvement. *Polym Int*. 2014;63:848–857.
18. Konkolewicz D, Wang Y, Zhong M, Krys P, Isse AA, Gennaro A, Matyjaszewski K. Reversible-deactivation radical polymerization in the presence of metallic copper. A critical assessment of the SARA ATRP and SET-LRP mechanisms. *Macromolecules*. 2013;46:8749–8772.
19. Zhong M, Wang Y, Krys P, Konkolewicz D, Matyjaszewski K. Reversible-deactivation radical polymerization in the presence of metallic copper. Kinetic simulation. *Macromolecules*. 2013;46:3816–3827.
20. Zhou Y-N, Luo Z-H. Copper(0)-mediated reversible-deactivation radical polymerization: kinetics insight and experimental study. *Macromolecules*. 2014;47:6218–6229.
21. Haehnel AP, Fleischmann S, Hesse P, Hungenberg K-D, Barner-Kowollik C. Investigating Cu(0)-mediated polymerizations: new kinetic insights based on a comparison of kinetic modeling with experimental data. *Macromol React Eng*. 2013;7:8–23.
22. Tasdelen MA, Uygun M, Yagci Y. Studies on photoinduced ATRP in the presence of photoinitiator. *Macromol Chem Phys*. 2011;212:2036–2042.
23. Tasdelen MA, Ciftci M, Yagci Y. Visible light-induced atom transfer radical polymerization. *Macromol Chem Phys*. 2012;213:1391–1396.
24. Zhang T, Chen T, Amin I, Jordan R. ATRP with a light switch: photoinduced ATRP using a household fluorescent lamp. *Polym Chem*. 2014;5:4790–4796.
25. Zhou Y-N, Luo Z-H. An old kinetic method for a new polymerization mechanism: toward photochemically mediated ATRP. *AIChE J*. 2015;61:1947–1958.
26. Magenau AJD, Strandwitz NC, Gennaro A, Matyjaszewski K. Electrochemically mediated atom transfer radical polymerization. *Science*. 2011;332:81–84.
27. Bortolamei N, Isse AA, Magenau AJD, Gennaro A, Matyjaszewski K. Controlled aqueous atom transfer radical polymerization with electrochemical generation of the active catalyst. *Angew Chem Int Ed*. 2011;50:11391–11394.
28. Magenau AJD, Bortolamei N, Frick E, Park S, Gennaro A, Matyjaszewski K. Investigation of electrochemically mediated atom transfer radical polymerization. *Macromolecules*. 2013;46:4346–4353.
29. Li B, Yu B, Huck WTS, Zhou F, Liu W. Electrochemically induced surface-initiated atom-transfer radical polymerization. *Angew Chem Int Ed*. 2012;51:5092–5095.
30. Li B, Yu B, Huck WTS, Liu W, Zhou F. Electrochemically mediated atom transfer radical polymerization on nonconducting substrates: controlled brush growth through catalyst diffusion. *J Am Chem Soc*. 2013;135:1708–1710.
31. Park S, Cho HY, Wegner KB, Burdynska J, Magenau AJD, Paik HJ, Jurga S, Matyjaszewski K. Star synthesis using macroinitiators via electrochemically mediated atom transfer radical polymerization. *Macromolecules*. 2013;46:5856–5860.
32. Park S, Chmielarz P, Gennaro A, Matyjaszewski K. Simplified electrochemically mediated atom transfer radical polymerization using a sacrificial anode. *Angew Chem Int Ed*. 2015;127:2418–2422.
33. Liu WF, Guo S, Fan H, Wang WJ, Li BG, Zhu SP. Synthesis of ethylene/1-octene copolymers with controlled block structure by semibatch living copolmerization. *AIChE J*. 2013;59:4686–4695.
34. Liu SJ, Cao K, Yao Z, Li BG, Zhu SP. Model development for semicontinuous production of ethylene and norbornene copolymers having uniform composition. *AIChE J*. 2009;55:663–674.
35. Zhou Y-N, Luo Z-H. Insight into the ATRP rate controlling ability of initiator structure: micromolecular, macromolecular, and immobilized initiators. *J Polym Sci Part A Polym Chem*. 2014;52:2228–2238.
36. D'hooge DR, Reyniers M-F, Stadler FJ, Dervaux B, Bailly C, Du Prez FE, Marin GB. Atom transfer radical polymerization of isobornyl acrylate: a kinetic modeling study. *Macromolecules*. 2010;43:8766–8781.
37. Tang W, Matyjaszewski K. Kinetic modeling of normal ATRP, normal ATRP with [CuII] 0, reverse ATRP and SR&NI ATRP. *Macromol Theory Simul*. 2008;17:359–375.
38. Zhu S. Modeling of molecular weight development in atom transfer radical polymerization. *Macromol Theory Simul*. 1999;8:29–37.
39. Wang R, Luo Y, Li BG, Zhu S. Control of gradient copolymer composition in ATRP using semibatch feeding policy. *AIChE J*. 2007;53:174–186.
40. D'hooge DR, Reyniers M-F, Marin GB. Methodology for kinetic modeling of atom transfer radical polymerization. *Macromol React Eng*. 2009;3:185–209.
41. Ribelli TG, Konkolewicz D, Bernhard S, Bernhard S, Matyjaszewski K. How are radicals (re)generated in photochemical ATRP? *J Am Chem Soc*. 2014;136:13303–13312.
42. Asua JM, Beuermann S, Buback M, Castignolles P, Charleux B, Gilbert RG, Hutchinson RA, Leiza JR, Nikitin AN, Vairon J-P, van Herk AM. Critically evaluated rate coefficients for free-radical polymerization. *Macromol Chem Phys*. 2004;205:2151–2160.
43. Nikitin AN, Hutchinson RA, Buback M, Hesse P. Determination of intramolecular chain transfer and midchain radical propagation rate coefficients for butyl acrylate by pulsed laser polymerization. *Macromolecules*. 2007;40:8631–8641.
44. Konkolewicz D, Sosnowski S, D'hooge DR, Szymanski R, Reyniers M-F, Marin GB, Matyjaszewski K. Origin of the difference between branching in acrylates polymerization under controlled and free radical conditions: a computational study of competitive processes. *Macromolecules*. 2011;44:8361–8373.
45. Fischer H, Paul H. Rate constants for some prototype radical reactions in liquids by kinetic electron spin resonance. *Acc Chem Res*. 1987;20:200–206.
46. Plessis C, Arzamendi G, Leiza JR, Schoonbrood HAS, Charmot D, Ausa JM. Modeling of seeded semibatch emulsion polymerization of n-BA. *Ind Eng Chem Res*. 2001;40:3883–3894.
47. Peck ANF, Hutchinson RA. Secondary reactions in the high-temperature free radical polymerization of butyl acrylate. *Macromolecules*. 2004;37:5944–5951.
48. Delgadillo-Velazquez O, Vivaldo-Lima E, Quintero-Ortega IA, Zhu S. Effects of diffusion-controlled reactions on atom-transfer radical polymerization. *AIChE J*. 2002;48:2597−2608.
49. D'hooge DR, Reyniers MF, Marin GB. The crucial role of diffusional limitations in controlled radical polymerization. *Macromol React Eng*. 2013;7:362–379.
50. Derboven P, D'hooge DR, Reyniers M-F, Marin GB, Barner-Kowollik C. The long and the short of radical polymerization. *Macromolecules*. 2015;48:492–501.
51. Rabea AM, Zhu S. Modeling the influence of diffusion-controlled reactions and residual termination and deactivation on the rate and control of bulk ATRP at high conversions. *Polymers*. 2015;7:819–835.
52. Bard AJ, Faulkner LR. *Electrochemical Methods: Fundamentals and Applications*, *2nd ed*. New York: Wiley, 2001.
53. Tang W, Tsarevsky NV, Matyjaszewski K. Determination of equilibrium constants for atom transfer radical polymerization. *J Am Chem Soc*. 2006;128:1598–1604.
54. Braunecker WA, Tsarevsky NV, Gennaro A, Matyjaszewski K. Thermodynamic components of the atom transfer radical polymerization equilibrium: quantifying solvent effects. *Macromolecules*. 2009;42:6348–6360.
55. Horn M, Matyjaszewski K. Solvent effects on the activation rate constant in atom transfer radical polymerization. *Macromolecules*. 2013;46:3350–3357.
56. Payne KA, Cunningham MF, Hutchinson RA. ARGET ATRP of BMA and BA: exploring limitations at low copper levels. *ACS Symp Ser*. 2012;1100:183–202.
57. Wang Y, Soerensen N, Zhong M, Schroeder H, Buback M, Matyjaszewski K. Improving the "livingness" of ATRP by reducing Cu catalyst concentration. *Macromolecules*. 2013;46:683–691.
58. Zhou Y-N, Luo Z-H, Chen J-H. Theoretical modeling coupled with experimental study on the preparation and characteristic comparison of fluorinated copolymers: effect of chain structure on copolymer properties. *AIChE J*. 2013;59:3019–3033.

Manuscript received May 16, 2015, and revision received July 4, 2015.